Climate Services 5 (2017) 23–35

Contents lists available at ScienceDirect

Climate Services

journal homepage: www.elsevier.com/locate/cliser

Future projections of extreme precipitation intensity-duration-frequency curves for climate adaptation planning in New York State

Arthur T. DeGaetano *, Christopher M. Castellano

Northeast Regional Climate Center, Department of Earth and Atmospheric Sciences, Cornell University, Ithaca, NY 13068, United States

ARTICLE INFO

Article history:
Received 22 August 2016
Received in revised form 21 December 2016
Accepted 14 March 2017
Available online 31 March 2017

Keywords:
Extreme rainfall
CMIP5
Downscaling
Intensity-duration-frequency curves

ABSTRACT

A set of future extreme precipitation probabilities are developed for New York State based on different downscaling approaches and climate model projections. Based on nearly 50 downscaling method-climate model combinations, percent differences are computed between simulated extreme precipitation amounts for one historical (1970–1999) and three future (2010–2039, 2040–2069, and 2070–2099) time periods. These percent change factors are then applied to the observed extremes to estimate future precipitation extremes. The results are presented to users via an interactive website (http://ny-idf-projections.nrcc.cornell.edu). As the engineering community is the primary user, the website displays intensity-duration-frequency (IDF) graphs depicting the: 1) mean projected extreme precipitation intensity, 2) range of future model projections, 3) distribution of observed extreme precipitation intensities, 4) confidence intervals about the observed values.

One-hundred-year recurrence interval precipitation amounts exhibit a median increase of between 5 and 10% across the state in the 2010–2039 period regardless of greenhouse gas concentration. By the 2040–2069 period, the median increase is on the order of 10–20% for the high concentration case (RCP 8.5), but remains below 10% if concentrations are lower (RCP 4.5). At the end of the century, all downscaling method climate model combinations indicate increases, with a median change of between 20 and 30% in the case of high concentrations.

Practical Implications

In 2014, New York State (NYS) enacted the Community Risk and Resiliency Act (CRRA). This act requires applicants (e.g. local communities) as well as state agencies to consider future flood risk in planning and constructing public infrastructure. State agencies must also consider these hazards in funding or permitting decisions. Although CRRA mandates consideration of future climate risks, it offers no implementation guidance. Rather, CRRA requires the NYS Department of Environmental Conservation (DEC) to develop such guidance.In addition to sea-level rise, NYS views effective implementation of the CRRA as dependent on projections of future extreme precipitation frequency. Current design standards for hydrologic and transportation infrastructure, as well as public and environmental safety regulations, are based on historical precipitation recurrence probabilities. An underlying assumption of these extreme precipitation analyses has been the stationarity of the historical record. Recently the validity of this assumption has been called into question, as numerous studies have shown a significant increase in the frequency and magnitude of extreme precipitation across the northeastern United States since the mid-20th century.This work describes the development of a set of future precipitation recurrence probabilities for NYS using a set of nearly 50 downscaled climate model projections. Based on different statistical or dynamical downscaling approaches and different global climate models, percent differences were computed between simulated extreme precipitation amounts for one historical (1970–1999) and three future (2010–2039, 2040–2069, and 2070–2099) time periods. These percent change factors were then applied to the observed extremes to estimate future precipitation extremes. An ensemble mean value and range (10th–90th percentile) of future projections were obtained from the set of climate model-downscaling method combinations.An interactive website (http://ny-idf-projections.nrcc.cornell.edu) facilitates access of the results by the user community, with products tailored to both engineers and less technical users. Station-specific intensity-duration-frequency (IDF) graphs

* Corresponding author at: Northeast Regional Climate Center, 1119 Bradfield Hall, Ithaca, NY 14853, United States.
E-mail address: atd2@cornell.edu (A.T. DeGaetano).

http://dx.doi.org/10.1016/j.cliser.2017.03.003
2405-8807/

(Fig. 10) provide the data necessary for engineering applications to demonstrate consideration of future climate conditions. The IDF graphs present four key pieces of information: 1) mean projected extreme precipitation intensity in future time periods, 2) a measure of variability in the future model projections; 3) historical extreme precipitation statistics based on station data; and 4) confidence intervals illustrating the uncertainty inherent to historical values. This allows users to weigh the future changes relative to a range of equally plausible precipitation extremes based on historical data.Complementary map-based products offer non-technical users a cursory statewide view of the projected changes in extreme precipitation. The results show that continued increases in extreme precipitation are expected across NYS, with little spatial variability in the magnitude of percent change relative to historical precipitation extremes. In the early part of the 21st century, the average increase in recurrence interval precipitation amounts is typically 5–10% (Fig 6a) with considerable overlap between the historical confidence intervals and range of future model projections. By mid-century (2040–2069), increases are generally in the 10–20% range assuming continued high greenhouse gas concentrations (Fig 6b). The late-century (2070–2099) estimates show the most model-to-model variability with increases averaging between 15–25% (Fig. 6c), but exceeding 50% at some stations. By late century, precipitation intensities that currently have a 1% chance of occurring in any year are expected to occur at least twice as frequently across much of the state (Fig. 11).

1. Introduction

Extreme precipitation has important implications for urban and rural development, public infrastructure, watershed management, agriculture, and human health. Historical climate records indicate that the northeastern U.S. has experienced significant increases in extreme precipitation since the mid-to-late twentieth century (DeGaetano, 2009; Heineman, 2012; Kunkel et al., 1999; Kunkel, 2003). Moreover, the most recent assessment from the Intergovernmental Panel on Climate Change (IPCC, 2014) reports with likely confidence that the frequency and magnitude of extreme precipitation in this region will continue to increase throughout the twenty-first century. Such changes will exacerbate the societal impacts of extreme precipitation in the future.

The Northeast U.S. is not the only region that has been experiencing greater extreme precipitation frequency and magnitude. Similar trends are noted in the central U.S. (Groisman et al., 2012) as well as many other regions throughout the world (Groisman et al., 2005; Fischer and Knutti, 2016). Other measures of extreme precipitation, such as maximum 5-day accumulation and precipitation amount on extremely wet days, have also shown increasing trends in the U.S., Europe, and Australia (Janssen et al., 2014; Moberg and Coauthors, 2006; Alexander and Arblaster, 2009). Other recent examples in the literature demonstrate the extent to which extreme precipitation has increased from both regional (e.g. Scherrer et al., 2016; Limsakul and Singhruck, 2016) and global (e.g. Donat et al., 2016) perspectives. Coumou and Rahmstorf (2012) point to increases in atmospheric water vapor (consistent with increasing average temperature) and increases in the frequency of local convective storm events (also enhanced by warming surface temperatures) as physical reasons for these changes. However, in some regions, linkages to certain atmospheric circulation patterns have been posed as influencing changes in precipitation extremes (e.g. Kenyon and Hegerl, 2010). Climate model simulations suggest a continuation of these extreme precipitation trends through the 21st century (e.g. Donat et al., 2016; Ning et al., 2015; Sun et al., 2016).

Engineering design has long relied on statistical extreme value analysis of precipitation (Yarnell, 1935). Intensity duration frequency (IDF) curves typically serve as a conduit for translating precipitation to runoff volume, particularly in basins under 65 km^2. These curves specify precipitation intensity ($mm\ hr^{-1}$) as a function of storm duration and average return frequency.

An underlying assumption of traditional IDF analyses has been stationarity of the climate. Hence, it was expected that past conditions were an adequate guide to the future. However, given the many studies documenting observed and projected increases in extreme precipitation frequency, decision makers have begun to question this assumption and seek information regarding projected future extreme precipitation frequency. Most efforts to estimate future IDF information have been on a case-by-case basis, often at the city level. This is quite different from historical extreme precipitation analyses that have typically been published at broad national or regional scales (e.g. Perica et al., 2013). Likewise, existing IDF projections have been developed by a range of climate service providers ranging from government and academia to the private sector, as opposed to historical analyses that have been almost exclusively developed by government agencies and then applied to specific locations or projects by the consulting industry.

An example of city-level IDF projections (AMEC Environment Infrastructure, 2012) uses the generalized linear model approach of Towler et al. (2010) to estimate future IDF values for Welland, Ontario, Canada using climate model output as predictors. Relative to the existing Welland IDF curve that was compiled in 1963, they found that precipitation intensities on average decrease through 2050. Wang et al. (2015) developed projected IDF curves for other cities in Ontario, Canada, using dynamically downscaled precipitation data from a regional climate modeling system (PRECIS; Wilson et al., 2011) driven by an ensemble of Hadley Centre Coupled Model, version 3 (HadCM3) output. They found that projected 24-h 100-year precipitation amounts increased by about 25% from the historical base period to the 2080s. Rodríguez et al. (2014) used a statistical downscaling approach to investigate changes in IDF curves for Barcelona, Spain. They found projected increases in precipitation extremes of between 3 and 14% by the late 21st century for recurrence intervals ranging from 10 to 500 years.

This paper discusses a project designed to provide NYS with guidance regarding plausible future changes in extreme precipitation return frequency. One of the impetuses for this work is the Climate Risk and Resiliency Act (CRRA), which requires specific state permitting, funding and regulatory decisions to demonstrate that future climate risks associated with flooding (inland, storm surge and sea level rise) have been taken into account. Currently, approaches for addressing future flood risk are not well defined. Suggestions range from the use of the 1% annual flood elevation plus an additional 0.61 m (2 ft) of freeboard to the use of the 0.2% annual recurrence (500-yr) flood (Lowery, personal communication, 2016). NYS prefers a climate-informed science approach that relies on projections of future precipitation-intensity frequencies for different durations. This paper describes the approach used to achieve this goal including 1) evaluation of downscaling method–climate model combinations in replicating historical precipitation extremes, 2) application of downscaling methods to project precipitation extremes in future periods, 3) quantification of methodological and climate model uncertainties, and 4) dissemination of results to users via web-based tools.

2. Data

2.1. Observed station data

To coincide with existing extreme precipitation climatologies (e.g. Perica et al., 2013), a set of 157 long-term Global Historical Climate Network (GHCN) stations (Menne et al., 2012) located in and adjacent to New York were the primary data source (Fig. 1). These daily data were obtained via the Applied Climate Information System (ACIS) supported by the Northeast Regional Climate Center (DeGaetano et al., 2015). Stations were required to have valid precipitation observations (i.e. not missing or flagged by GHCN quality control) on at least 95% of all days during the 1961–2010 period. To achieve a higher station density, the valid data criterion was relaxed to 85% to include sites located more than 25 km from those with 95% data availability and subsequently a few stations with at least 75% data availability were included if they were located more than 25 km from the others.

2.2. Gridded data sources

Historical and future atmosphere–ocean general circulation model (AOGCM) and Earth System model (ESM) output was obtained from two sources. Simulations from the models' historical period and two future Representative Concentration Pathways (RCP4.5 and RCP 8.5) (Collins, 2013) were used. At the global scale, daily precipitation simulations from 25 models (Table 1) included in Phase 5 of the Coupled Model Intercomparison Project (CMIP5) (Taylor et al., 2012) were downloaded from http://pcmdi9.llnl.gov. In addition to daily precipitation output, 6-hourly specific humidity, zonal wind and meridional wind fields were obtained from 20 CMIP5 models. These variables were necessary to compute 850-hPa relative vorticity (ζ_{850}), total precipitable water (TPW), and vertically integrated water vapor transport (IVT) for analog-method (Castellano and DeGaetano, 2015) downscaling.

Daily precipitation simulations from the Coordinated Regional Climate Downscaling Experiment (CORDEX; Jones et al., 2011), were also obtained from the website https://na-cordex.org. The CORDEX simulations consist of regional climate models (RCMs) run at approximately 50-km resolution and driven by AOGCMs or ESMs from CMIP5. Four CORDEX model combinations are currently available for the North American domain.

To construct the set of historical precipitation extremes needed for analog-method downscaling, the necessary 6-hourly variables were obtained or computed from the National Centers for Environmental Prediction–National Center for Atmospheric Research (NCEP–NCAR) Reanalysis (Kalnay and Coauthors, 1996). The NCEP–NCAR reanalysis data are available at 2.5° × 2.5° horizontal resolution and 17 vertical pressure levels between 1000-hPa and 10-hPa. The utilization of the NCEP-NCAR Reanalysis data allows for gridded comparison between CMIP5 patterns and historical analog patterns.

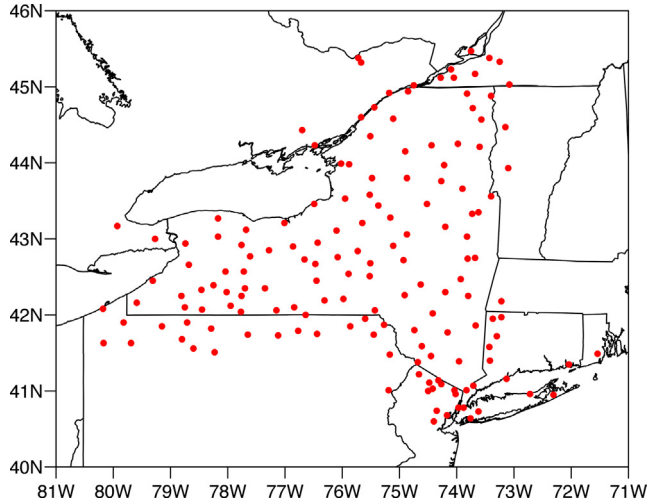

Fig. 1. Global Historical Climatology Network stations in New York and surrounding areas of adjacent states and Canada.

Table 1
List of CMIP5 models used.

CMIP5 Model ID	Modeling Center/Group	Resolution
ACCESS1.0*	CSIRO, Australia	1.25° × 1.875°
ACCESS1.3*	CSIRO, Australia	1.25° × 1.875°
BCC–CSM1.1	Beijing Climate Center, China	1.125° × 1.125°
BCC–CSM1.1(m)	Beijing Climate Center, China	2.8° × 2.8°
BNU–ESM	Beijing Normal University, China	2.8° × 2.8°
CCSM4	National Center for Atmos. Research, USA	0.9° × 1.25°
CMCC–CM*	Euro–Mediterranean Centre on Climate Change, Italy	0.75° × 0.75°
CNRM–CM5	National Centre for Meteorological Research, France	1.4° × 1.4°
CSIRO–Mk3.6.0	CSIRO, Australia	1.875° × 1.875°
CanESM2	Canadian Centre for Climate Modeling and Analysis, Canada	1.875° × 1.875°
FGOALS–g2*	LASG, China	2.8° × 2.8°
GFDL–CM3	Geophysical Fluid Dynamics Lab, USA	2.0° × 2.5°
GFDL–ESM2 G	Geophysical Fluid Dynamics Lab, USA	2.0° × 2.5°
GFDL–ESM2 M	Geophysical Fluid Dynamics Lab, USA	2.0° × 2.5°
GISS–E2–H	NASA Goddard Inst. for Space Sci., USA	2.0° × 2.5°
GISS–E2–R	NASA Goddard Inst for Space Sci, USA	2.0° × 2.5°
HADGEM2–ES*	Met Office Hadley Centre, United Kingdom	1.25° × 1.875°
IPSL–CM5A–LR	Pierre Simon Laplace Institute, France	1.9° × 3.75°
IPSL–CM5A–MR	Pierre Simon Laplace Institute, France	1.25° × 2.5°
IPSL–CM5B–LR	Pierre Simon Laplace Institute, France	1.9° × 3.75°
MIROC–ESM	JAMSTEC/AORI/NIES, Japan	2.8° × 2.8°
MIROC–ESM–CHEM	JAMSTEC/AORI/NIES, Japan	2.8° × 2.8°
MIROC5	JAMSTEC/AORI/NIES, Japan	1.4° × 1.4°
MRI–CGCM3	Meteorological Research Institute, Japan	1.125° × 1.125°
NorESM1–M	Norwegian Climate Center, Norway	1.9° × 2.5°

* These models were used for the quantile delta method but not the analog method.

3. Extreme value analysis

Recurrence interval precipitation amounts were computed based on partial duration series (PDS) of the n largest independent daily precipitation events, where n is the number of years in the station record (Wilks and Cember, 1993). To be considered independent, chronologically successive PDS events had to be separated by at least seven days (Xuereb and Green, 2012). For the station data and the historical climate model simulations, PDS spanned the 1970–1999 period (n = 30). For consistency, PDS for future time periods were also limited to 30 years. Periods of 30 years also characterized the shortest observational records used in current extreme precipitation analyses.

After PDS were constructed for each station, precipitation amounts corresponding to 2-, 5-, 10-, 25-, 50-, and 100-year recurrence intervals were computed using two statistical fitting approaches. The first approach, hereafter referred to as Beta-P, employs the Levenberg-Marquardt method (Press et al., 1986) of maximum likelihood estimation to fit the Beta-P distribution (Mielke and Johnson, 1974) to each station's PDS. Wilks (1993) examined several candidate probability distributions for estimating precipitation extremes and concluded that the Beta-P distribution best captured the extreme right tail of precipitation events in the northeastern U.S.

The second approach, hereafter referred to as L-moments, first groups stations based on similarities in their extreme precipitation distributions, and then applies L-moments regional frequency analysis (Hosking and Wallis, 1997) to compute recurrence interval amounts. Station groups were determined by running two-sample Kolmogorov–Smirnov tests on the PDS cumulative distribution functions at different pairs of stations (DeGaetano, 1998). The generalized extreme value (GEV) distribution was fit to each station's PDS, with regionally averaged shape and scale parameters specified for all stations in a given group. The U.S National Weather Service (NWS) is currently using a similar L-moments approach to create revised (observed) precipitation-frequency atlases for regions within the U.S. (Perica et al., 2013). As Fig. 2 suggests, the Beta-P and L-moments approaches yield very similar values at shorter recurrence intervals, but at longer return periods, larger differences emerge. In particular, the GEV-based L-moments values at longer recurrence intervals are typically lower than the Beta-P values, as expected based on Wilks (1993). Maps showing the current observed geographic patterns of extreme rainfall recurrence frequencies can be viewed at http://precip.net or http://hdsc.nws.noaa.gov/hdsc/pfds/pfds_maps.html .

When computing extreme precipitation statistics it is important to recognize that there are several inherent sources of uncertainty. In addition to the choice of theoretical extreme value distribution and fitting technique, the assumption that the PDS sample reflects the true population of extreme precipitation events leads to uncertainty in the computation of recurrence interval precipitation amounts. This is exacerbated by differences in the available data records among stations (Ward et al., 2015). To quantify this source of uncertainty, a resampling approach was used. For each station's n-year PDS, n precipitation amounts were randomly selected with replacement 1000 times. After computing the Beta-P and L-moments recurrence interval precipitation amounts for each of these 1000 trials, the 5th and 95th percentiles were determined for each recurrence interval to represent lower and upper confidence interval bounds.

Based on the fitted daily precipitation extremes, IDF curves were formulated. User requirements necessitated that the IDF curves include 1-, 2-, 3-, 6-, 12-, 18-, and 24-h duration precipitation intensities. Sub-daily recurrence interval precipitation amounts were estimated by applying empirical adjustment factors to the daily recurrence interval precipitation amounts (McKay and Wilks, 1995). Thus, future changes in sub-daily precipitation amounts are proportional to the projected changes in daily precipitation amounts.

The use of static adjustments is warranted based on the stability of empirical adjustments through time (and space) in the United States despite marked changes in daily extreme precipitation frequency (e.g. compare Hershfield, 1961 with Perica et al., 2013). Similarly, Palecki et al. (2005) found that 15-min rainfall intensity increased significantly only in winter, when few PDS rainfall events are observed. During other seasons, sub-daily rainfall trends during 1972–2002 showed a mix of non-significant increases and declines.

However, Westra et al. (2014) caution that rainfall intensity at sub-daily time scales may be more sensitive to increases in temperature than daily values. Unfortunately current global climate models are limited in their ability to simulate these time and space scales. This makes projections of sub-daily rainfall extremes uncertain. Recent studies examining sub-daily precipitation intensities using regional climate models show considerable variation. A case study for Sydney, Australia (Cortés-Hernández et al., 2015) showed that model-simulated sub-daily precipitation intensities underestimated the observations. Across Europe, the sign of future changes in sub-daily extreme precipitation varied regionally in RCM simulations (Scoccimarro et al., 2015). Users of the resulting projections

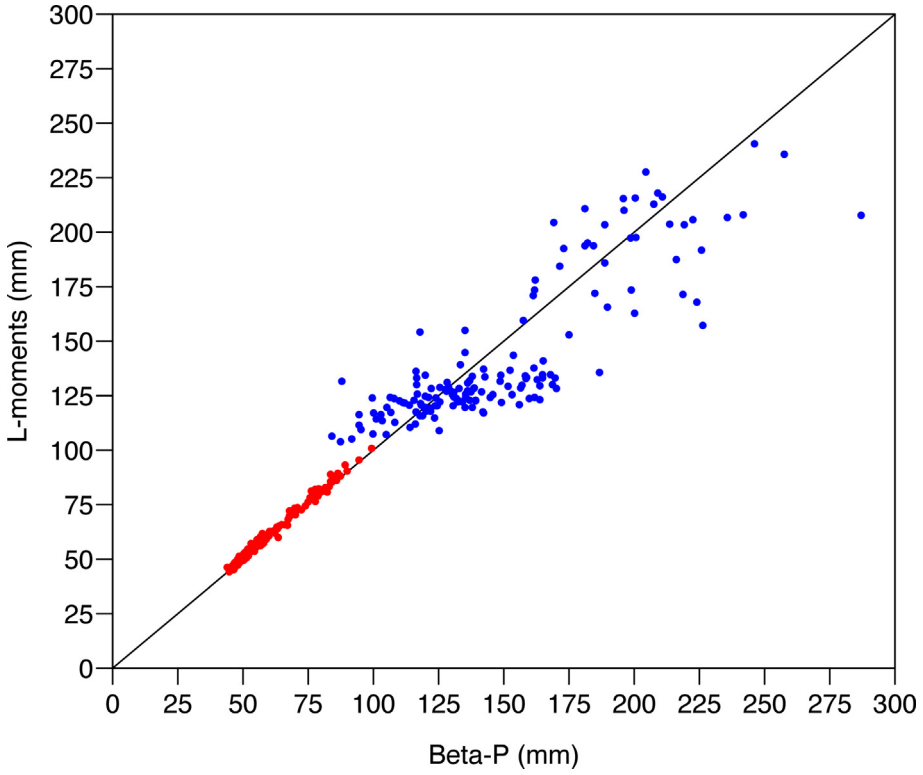

Fig. 2. Comparison of 2-year (red) and 100-year (blue) recurrence interval precipitation amounts at the 157 stations shown in Fig. 1 based on regional L-moments GEV fitting and maximum-likelihood Beta-P distribution fitting.

should be aware of these uncertainties and ideally require routine updates of the statistics based on additional data, refined model simulations, and increased scientific understanding.

A logarithmic regression was fit to the intensity–duration relationship to create smoothed IDF curves and interpolate recurrence interval precipitation amounts at intermediate durations. Upper and lower confidence interval IDF curves were smoothed in an analogous manner.

4. Downscaling

Since future IDF curves for individual stations were the main project deliverable, spatial downscaling was necessary to isolate station-scale climate information from the coarse-scale climate model output. For the purpose of this study, three different downscaling methods were applied. Both statistical and dynamical approaches were used.

4.1. Quantile delta method downscaling

The first downscaling method employs quantile delta mapping (Cannon et al., 2015) to estimate future precipitation extremes based on time-dependent changes in simulated CMIP5 precipitation extremes. Daily precipitation estimates at each station were interpolated from a weighted average of simulated daily precipitation over the four nearest grid cells. Grid cell weights were determined based on an inverse-distance-squared relationship. Next, PDS of the largest interpolated daily precipitation estimates at each station were constructed for the historical and future periods, and the Beta-P and L-moments approaches were used to compute the corresponding recurrence interval precipitation amounts. Due to the relatively coarse CMIP5 grid resolutions, no attempt was made to convert from areal to point precipitation values. Rather, future downscaled recurrence interval precipitation amounts were estimated by calculating the percent change in precipitation extremes between the interpolated historical and future periods, and then applying this factor to the observed precipitation extremes at the corresponding station.

In order to test the veracity of percent change factors computed in this manner, an upscaling experiment was conducted using output from the CORDEX simulations. The original 50-km resolution CORDEX output was aggregated to 100-, 150-, and 200-km grids by averaging sets of 4, 9, or 16 adjacent 50-km grid cell values, respectively. Results from this upscaling experiment suggest that grid cell resolution did not affect the magnitude of percent change.

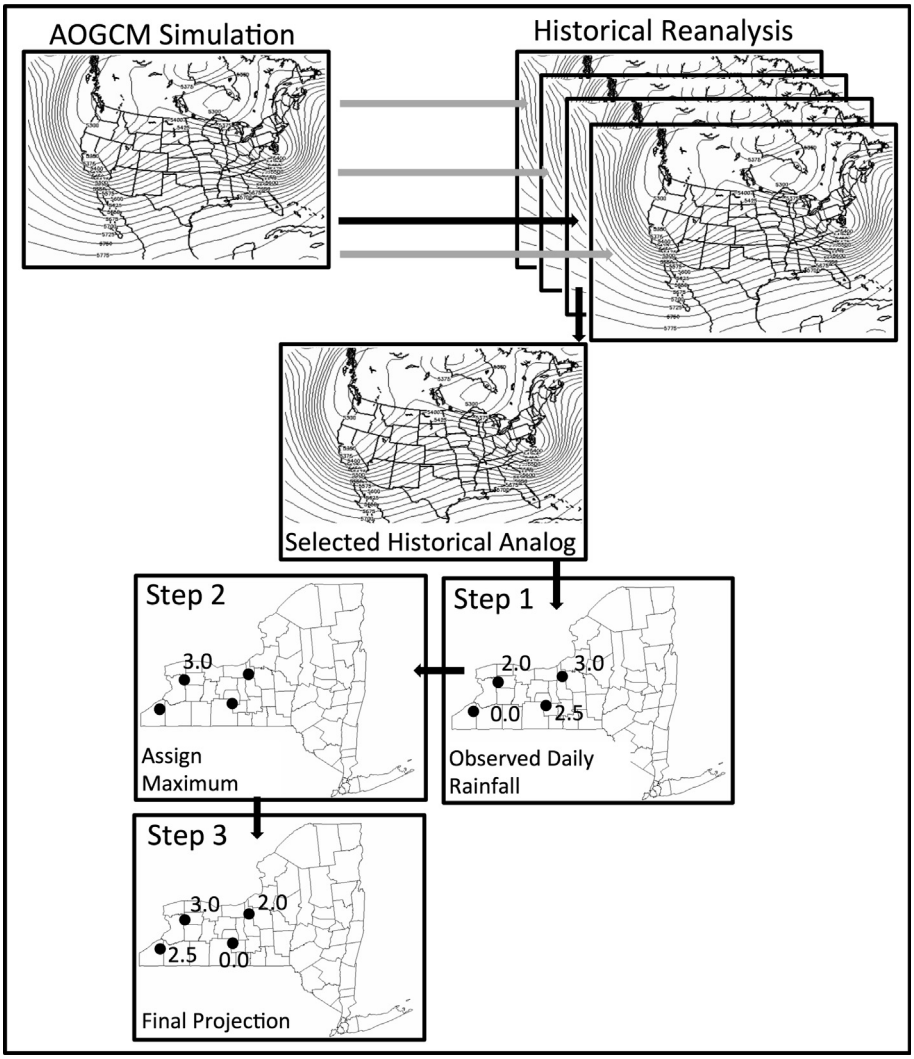

Fig. 3. Illustration of the analog downscaling method in which a single AOGCM simulation is paired with one of an array of potential historical analogs. Based on the observed precipitation pattern corresponding to the selected analog, the historical values are reassigned to obtain a future rainfall projection. The process is repeated for each daily AOGCM simulation.

While relevant to the specific variable (CORDEX precipitation) and region, this result should not be broadly applied to different geomorphological regions and/or variables.

4.2. Dynamic downscaling

The second downscaling method uses a simple bias correction technique to adjust dynamically downscaled precipitation extremes from the CORDEX simulations. As in the first method, daily precipitation estimates at each station were interpolated by an inverse-distance-squared-weighed average of simulated precipitation over the four closest CORDEX grid cells. PDS of the largest interpolated daily precipitation estimates at each station were constructed for the historical and future periods and the Beta-P and L-moments approaches were used to compute the corresponding recurrence interval precipitation amounts.

Because the simulated recurrence interval precipitation amounts were derived from daily precipitation totals averaged over 50-km grid cells, areal reduction factors (ARFs) were used to convert gridded precipitation to point values. For each return period, ARF was estimated by

$$\mathrm{ARF} = 1 - \exp\left(\mathrm{at}^{\mathrm{b}}\right) + \exp\left(\mathrm{at}^{\mathrm{b}} - \mathrm{cA}\right), \quad (1)$$

where t is the precipitation duration (hr), A is the grid area (1000 km^{-2}), and a, b, and c are empirically derived coefficients based on 24-h precipitation durations (Allen and DeGaetano, 2005).

Model biases were determined by computing the ratio of the ARF-adjusted recurrence interval precipitation amounts to the observed recurrence interval precipitation amounts during the historical period. Final future downscaled precipitation extremes were estimated by applying these bias correction factors to the ARF-adjusted future recurrence interval precipitation amounts with the assumption that model biases remain constant with time. This procedure is analogous to the quantile delta method discussed in the previous subsection, but allows for evaluation of historical biases.

4.3. Analog method

The third downscaling method employs an approach for downscaling daily precipitation extremes from historical analogs (Castellano and DeGaetano, 2015). Analog days were selected based on minimization of standardized root mean squared errors (RMSE) between predictor variables (ζ_{850}, TPW and IVT) from all days in the AOGCM simulations (hereafter AOGCM target days) and predictor variables on all candidate analog days spanning the 1961–2010 period (regardless of whether rainfall was observed). For the purpose of this study the RMSE calculation was restricted to the region bounded by 20°N, 105°W – 55°N, 50°W. These predictors represent synoptic-dynamic processes and thermodynamic environments commonly associated with heavy precipitation and flash flooding (Maddox et al., 1979; Doswell et al., 1996; Hirschboeck et al., 2000). Data fields for the historical analog days

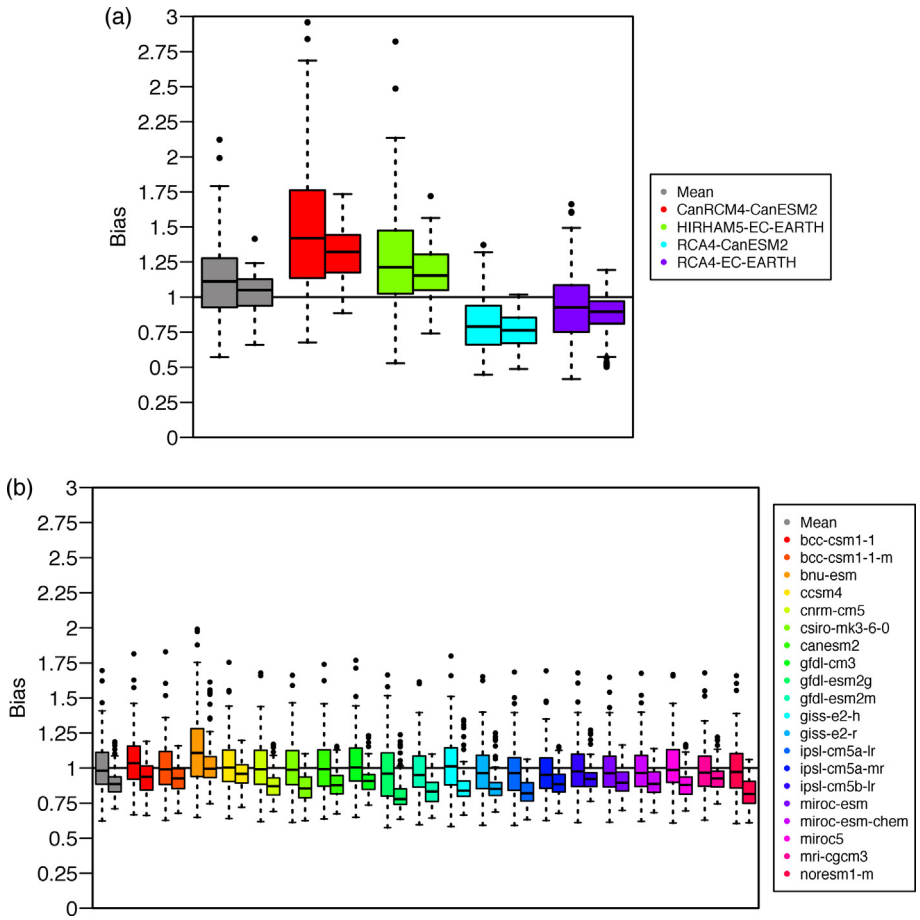

Fig. 4. Box-plots of bias (ratio of 100-year recurrence interval climate model precipitation to observed value) at 157 station locations for a) CORDEX simulations and b) CMIP5 model analog method downscaling. Box plot pairs show extreme values fit based the Beta-P (left) and L-moments approaches (right). The leftmost pair of boxplots (gray) shows the average over all simulations for the specific downscaling method.

were derived from 6-hourly NCEP–NCAR reanalysis, whereas the data fields on target days were derived from 6-hourly CMIP5 model output. For each daily AOGCM simulation, a single analog day was randomly selected from the pool of historical analogs corresponding to the 30 smallest RMSE values, with the probability of selection weighted by standardized RMSE (Fig. 3).

To translate the analog pattern to station precipitation, the 157 stations were first partitioned into five clusters based on how regularly different pairs of stations received extreme precipitation from the same meteorological event during the 1961–2010 period. Extreme precipitation was defined as the 50 largest precipitation events in the 1961–2010 period, separated by at least one week to assure independence. Defined in this way the set of extreme precipitation days formed the PDS commonly used in extreme rainfall frequency analysis. This cluster analysis accounted for the spatiotemporal variability in extreme precipitation across the study domain.

Then, it was determined if extreme precipitation occurred at any stations within each cluster on the selected analog day. If only one station in a specific cluster recorded a PDS event within a three-day window centered on the analog day, the corresponding daily precipitation amount was randomly assigned to one station in the cluster. The probability of assigning this precipitation amount to a station was quantified by isolating those daily events in which only one station in the cluster reported a PDS event during the 1961–2010 period and the computing the percentage of times that each specific station was represented in this subset.

If multiple stations in a cluster recorded a PDS event within the three-day window, each station's maximum daily precipitation observation over the three-day period was extracted (Fig. 3, Step 1), and these maximum daily precipitation observations were ascribed to all stations in the cluster in the following manner. The largest daily precipitation amount was always assigned separately based on each station's climatological probability of receiving the largest daily precipitation amount during a multi-station event to account for topographic effects (Fig. 3, Step 2). All remaining maximum daily precipitation amounts were randomly assigned with equal probability to the remaining stations in that cluster (Fig. 3, Step 3). If no stations in the cluster experienced a PDS event on the selected analog day, no precipitation amounts were assigned.

PDS constructed from the analog precipitation amounts were fit using the Beta-P and L-moments approaches to compute analog recurrence interval precipitation amounts. In order to minimize the effect of selecting one historical analog for each model day, the process of randomly selecting historical analogs, ascribing precipitation amounts, and computing recurrence interval precipitation amounts was repeated 1000 times. The median values of the 1000 Beta-P and L-moments precipitation extreme populations were chosen to represent the final downscaled precipitation threshold estimates. Similar to the dynamically downscaled projec-

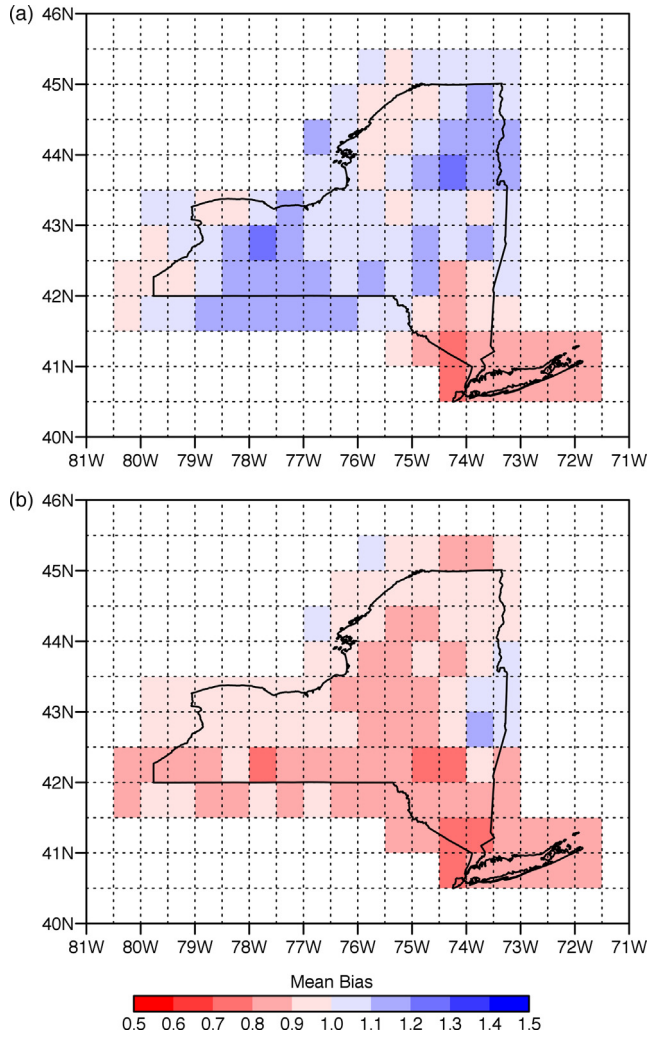

Fig. 5. Station specific a) CORDEX and b) analog method downscaling CMIP5 bias associated with the 100-year recurrence interval interpolated to a 0.5° × 0.5° grid.

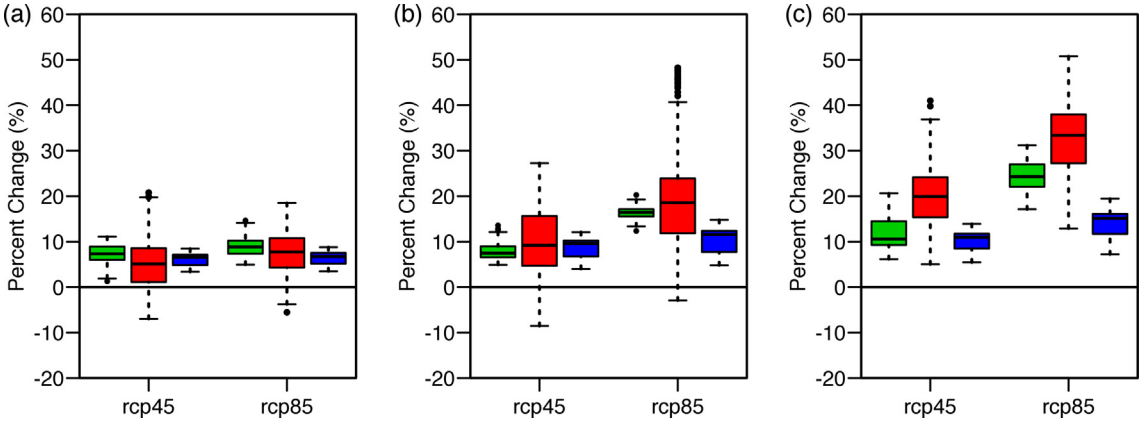

Fig. 6. Box-plots of mean percent change (modeled future period to model-simulated 1970–1999 historical period 100-year recurrence interval precipitation) based on quantile delta method (green), CMIP5 models downscaled using CORDEX (red), and analog approach (blue) for a) 2010–2039, b) 2040–2069 and c) 2070–2099. Boxplots represent the set of changes across 157 stations.

tions, the future downscaled precipitation extremes were adjusted by bias correction factors calculated from a comparison of the historical downscaled recurrence interval precipitation amounts and the observed recurrence interval precipitation amounts.

4.4. Quantifying uncertainty in downscaled projections

From the different downscaling method–climate model combinations, a set of 49 extreme precipitation projections (25 quantile method + 4 CORDEX + 20 analog method) was created at each station for each of the two climate scenarios and three time periods. For each set, the mean and 10th, 25th, 50th, 75th, and 90th percentiles were computed. These percentile values quantified the variability in future extreme precipitation projections among the climate model-downscaling method combinations.

5. Results

5.1. Historical bias

Before creating downscaled extreme precipitation projections for the future climate scenarios, the ability of each downscaling method–climate model combination to generate realistic estimates of observed recurrence interval precipitation amounts during the 1970–1999 period was assessed. Biases were computed as the ratio between the downscaled and observed recurrence interval precipitation amounts at each station for a specified return period. Fig. 4 shows boxplots of ensemble mean and individual model biases in 100-year recurrence interval precipitation amounts estimated from the dynamical and analog downscaling methods. Each boxplot characterizes the distribution of biases across the 157 stations. In general, the results for other recurrence intervals were similar.

Collectively, both downscaling methods yield realistic 100-year recurrence interval precipitation amounts at most stations (Fig. 4). However, pronounced differences exist between models and across stations. On average, the dynamical downscaling method overestimates recurrence interval precipitation amounts by approximately 5–10% (Fig. 4a), whereas the analog downscaling underestimates the precipitation extremes by a similar amount (Fig. 4b). On average, the L-moments approach consistently yields lower extreme values than the Beta-P approach and therefore moderates the biases associated with dynamic downscaling while exacerbating the analog method biases.

Due to the use of regionally averaged shape and scale parameters, L-moments biases exhibit substantially less station-to-station variability than the Beta-P biases. Particularly in the analog approach, the interquartile range of L-moments biases is often half that of the Beta-P biases (Fig. 4b). Additionally, the range of model biases computed from the Beta-P approach increases with return period (not shown), suggesting that the Beta-P approach is somewhat sensitive to return period length. This sensitivity is not apparent using the L-moments approach. Given this feature, as well as the use of the L-moments methodology in the official observed climatology of precipitation extremes (Perica et al., 2013), the L-moments approach was adopted in all future analyses.

Fig. 4 also illustrates the variation in extreme precipitation biases among the different models. For the analog method, there is as much as a 20% difference in median recurrence interval precipitation biases among the models. Using the L-moments approach, the Beijing Normal University Earth System Model (bnu esm) exhibits essentially no bias, whereas the Geophysical Fluid Dynamic Laboratory Earth System Model 2 g (gfdl esm2 g) and Norwegian Climate Centre Earth System Model 1 m (noresm1-m) underestimate the 100-year precipitation amount by nearly 20%. For the dynamically downscaled CORDEX simulations, the sign of the bias appears to be more related to the regional model used in downscaling as opposed to the driving earth system model (Fig 4a). Although the set of CORDEX simulations is currently limited, the two Rossby Centre regional climate model (RCA4) simulations tend to produce relatively small dry biases. Rel-

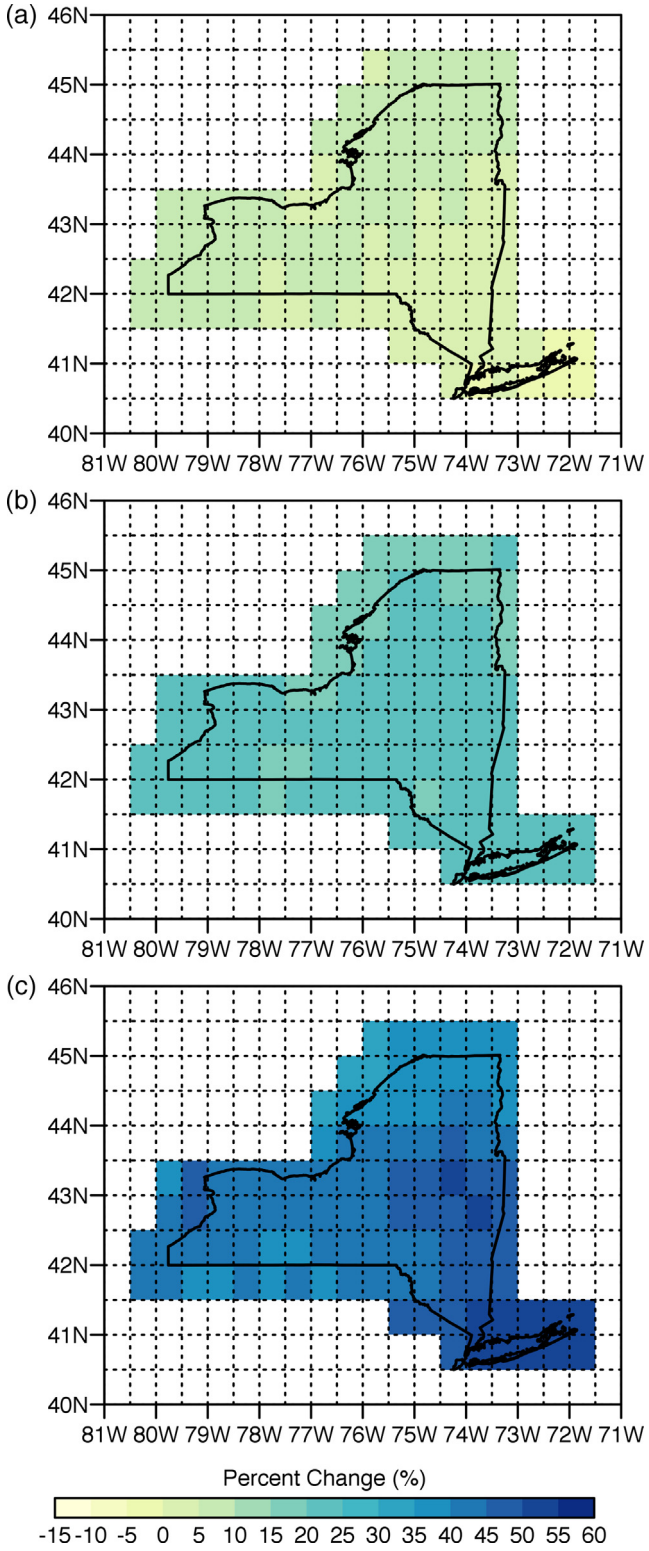

Fig. 7. Station-specific percent change (modeled RCP 8.5 2070–2099 period to model-simulated 1970–1999 historical period) interpolated to a 0.5° × 0.5° grid for the climate model –downscaling method combination yielding the a) 10th percentile b) average and c) 90th percentile percent change at each station.

atively smaller biases are also associated with the simulations driven by the European Consortium earth system model (EC-EARTH).

Fig. 5 illustrates the spatial variability of model mean bias in 100- year recurrence interval precipitation amounts. In this and subsequent figures, station values are interpolated to a 0.5° × 0.5° grid using the interp function (bilinear interpolation) in the matplotlib 1.0.8 toolkit http://matplotlib.org/basemap/api/basemap_api.html. The CORDEX simulations overestimate 100-year precipitation amounts throughout much of the state (Fig 5a), particularly in parts of western New York and over the mountainous northeastern region. Low (dry) biases are most pronounced in the coastal southeast across New York City and Long Island. By comparison, the analog downscaling method underestimates 100-year precipitation amounts across nearly the entire state (Fig. 5b). High biases are confined to the eastern part of the state. Biases are generally smallest in those areas where the CORDEX biases were largest.

5.2. Future projections

Fig. 6 summarizes the projected future percent change in 100-year model-mean precipitation amounts across all stations. Regardless of time period or concentration pathway, the dynamically downscaled CORDEX simulations exhibit the largest station-to-station variability. This is likely an artifact of the limited number of available CORDEX simulations, but may also be influenced by the higher resolution of the CORDEX data. For instance, only CORDEX simulations suggest that extreme precipitation may decrease at some stations during the early 21st century. Despite these projected decreases, the CORDEX simulations also project the largest increases throughout the mid-to-late 21st century (Fig. 6). By the end of the century, the CORDEX simulations project precipitation extremes to increase at all stations, with increases of 40–50% indicated at some locations. Station-to-station variability increases with time, regardless of downscaling approach.

In the 2010–2039 period, the 100-year precipitation amounts exhibit a median increase of between 5 and 10% across the 157 stations. The quantile delta and analog downscaling methods suggest increases at all stations, with the largest increase near 15%. The effect of greenhouse gas concentration appears to be minimal during this period.

By mid-century (2040–2069), the effect of concentration pathway becomes more pronounced. The median increase in 100-year precipitation amounts is less than 10% for all downscaling

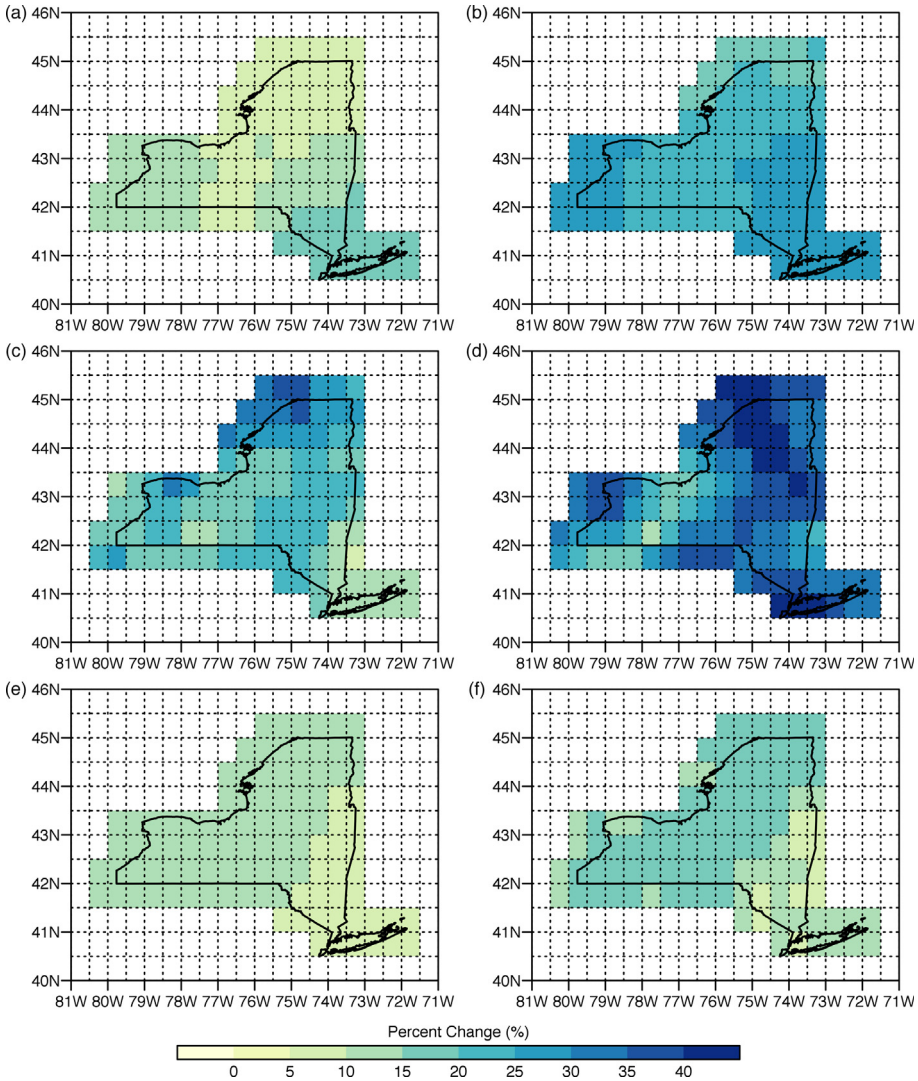

Fig. 8. Station-specific average percent change (modeled RCP 8.5 2070–2099 period to model-simulated 1970–1999 historical period) interpolated to a 0.5° × 0.5° grid for a) quantile delta simulations (RCP4.5); b) quantile delta simulations (RCP8.5); c) CORDEX simulations (RCP4.5); d) CORDEX simulations (RCP8.5); e) analog method simulations (RCP4.5); f) analog method simulations (RCP8.5).

methods under RCP4.5, but increases to 10–20% under the high concentration case (RCP8.5). Except for a few stations that still show decreases in extreme precipitation in the CORDEX simulations, on average the three downscaling approaches project similar changes under RCP4.5. Under RCP8.5, the different downscaling methods lead to more pronounced differences in the expected increase in precipitation extremes.

The differences between concentration pathways and downscaling methods are most pronounced in the 2070–2099 period. Regardless of downscaling method, 100-year precipitation amounts are expected to increase at all stations. Median changes range from 10–20% under RCP4.5, but vary considerably from 15% for the analog method to over 35% in the CORDEX simulations under RCP8.5. As in the RCP8.5 simulations during 2040–2069, there is a clear tendency for CORDEX simulations to produce the largest changes and the analog method to produce the smallest changes. For the RCP8.5 pathway in 2070–2099, there is no overlap of the interquartile ranges of the three downscaling methods.

As Fig. 7 illustrates, there is little consistency in the geographic variation in extreme precipitation change. Averaged across all climate model-downscaling method combinations, the projected change in 100-year recurrence interval extreme precipitation amounts by the 2070–2099 period (RCP 8.5) is between 15 and 25% statewide. For the 10th percentile change at each station, extreme precipitation changes tend to be smallest near the coast and largest inland to the north and west. Conversely, the spatial pattern of extreme precipitation change associated with each station's 90th percentile change suggests larger changes in the coastal southeast compared to the rest of the state.

Looking at the individual downscaling techniques, the quantile delta method produces the largest percentage changes in 100-year recurrence interval rainfall across southeastern NYS for the late-century simulations (Fig. 8a, b), but this pattern is not as evident for mid-century (Fig. 9a, b) period. The CORDEX simulations exhibit notably more grid-to- grid variation than the other downscaling methods and hence lack a consistent geographic pattern (Figs. 8c, d and 9c, d). Like the quantile-delta-method results, there is only modest consistency in the spatial pattern of projected changes across different concentration pathways and time periods. The analog method yields the most consistent spatial pattern of future change, with the smallest changes in southeastern New York and generally larger changes to the north and west (Figs. 8e, f and 9e, f). Attributing these findings to some aspect of the downscaling techniques is a goal of future research that is beyond the scope of this paper.

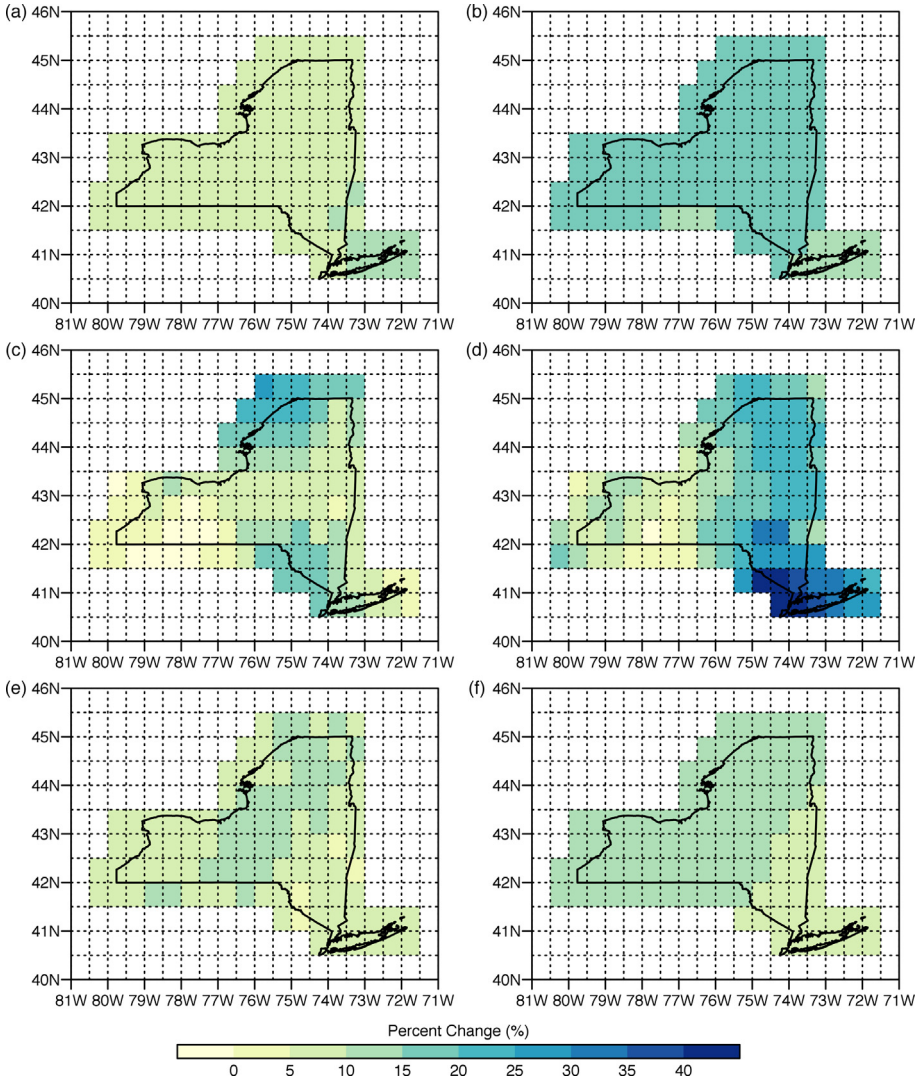

Fig. 9. As in Fig. 8, but for the 2040–2069 period.

6. Transition from research to application

To facilitate use by the engineering community in NYS, research results have been made accessible via an interactive website http://ny-idf-projections.nrcc.cornell.edu/. The primary tool used by engineers to develop design standards based on extreme precipitation statistics is the IDF curve. The IDF graph (Fig. 10) and accompanying tabular data relate precipitation duration (hours) to intensity (in/hr in the U.S.) for different recurrence intervals. The website presents a map interface showing station locations. Once a user selects a station by clicking one of the icons displayed on the map, the user is prompted to select a recurrence interval, concentration pathway, and a future time period. These selections change the IDF graphic and table displayed in the right column of the page.

The IDF curve that is displayed (Fig. 10) shows both the historical (based on observed precipitation) and projected future IDF curves. The two shaded regions illustrate uncertainty. The blue region in Fig. 10 shows the 90% confidence interval for the observed data derived from Monte-Carlo resampling of the observed PDS (DeGaetano, 2009). The red area is bounded by the 90th and 10th percentiles of the 49 climate model-downscaling method combinations. The decision to pool all of the projection combinations, was driven in part by stakeholder preference (desire for a single IDF graphic) but also by the patterns of downscaling method bias (Fig. 4) and the systematic differences in the magnitude of projected changes among the combinations (Fig. 6). Particularly for high concentrations and the later part of the century, the upper bound of the projection envelope typically corresponded to the CORDEX simulations while the lower bound was generally associated with the analog projections. Since the medians of the quantile delta and analog downscaling projections were similar (except for the late century RCP 8.5 simulations) the projected mean IDF curve in Fig. 10, reflects both of these downscaling approaches.

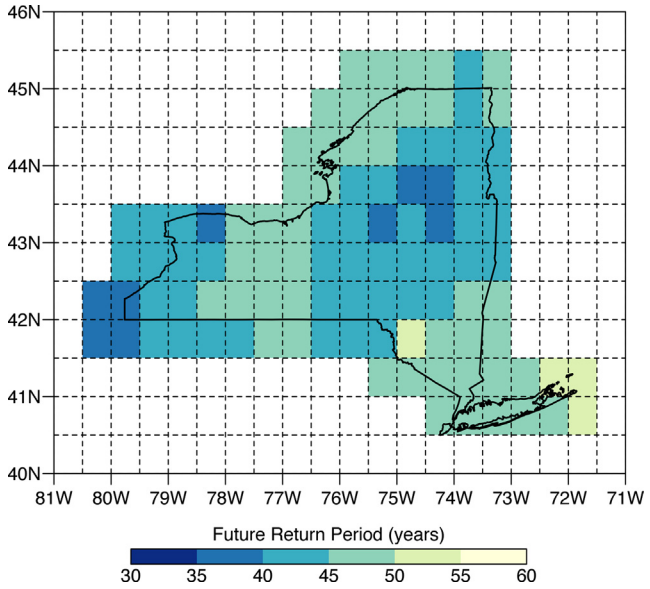

Fig. 11. Sample map-based product from the website http://ny-idf-projections.nrcc.cornell.edu/ showing projected (RCP 8.5) 2070–2099 recurrence intervals associated with the precipitation amounts that defined the 100-year recurrence interval storm in 1970–1999.

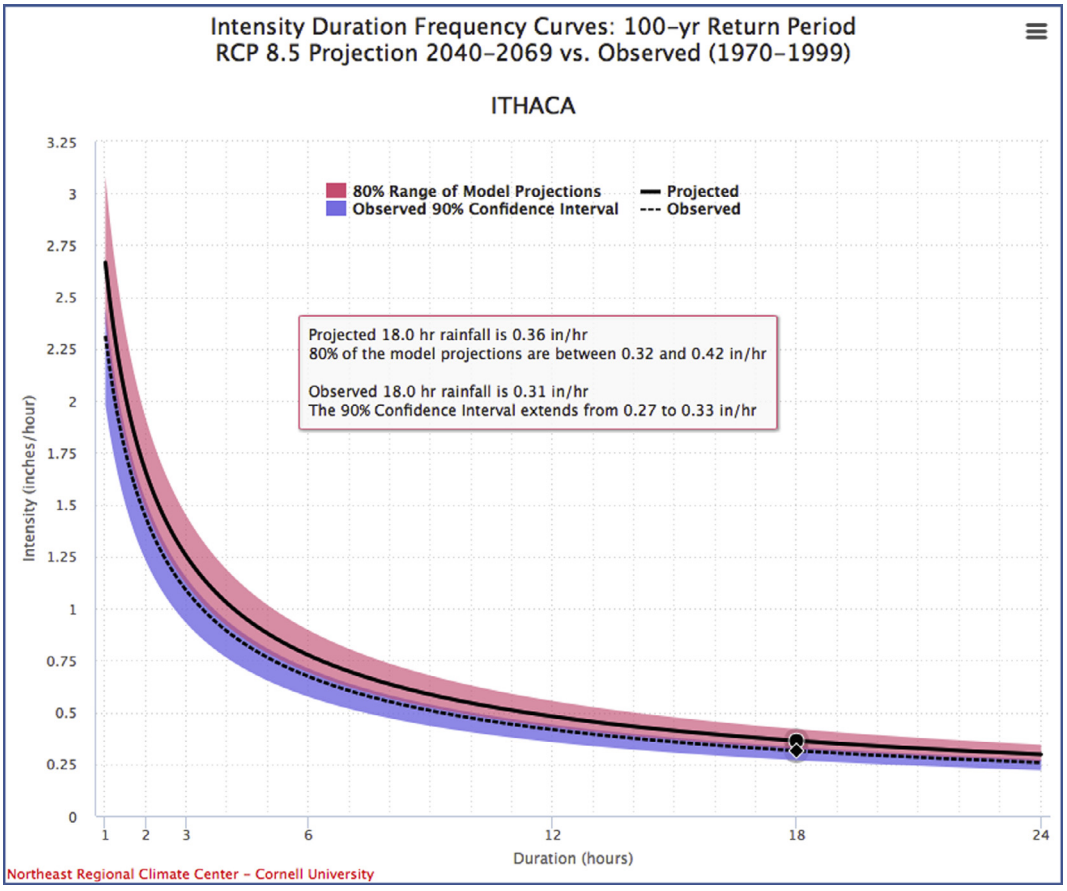

Fig. 10. Sample IDF curve product from the website http://ny-idf-projections.nrcc.cornell.edu/ showing historical and projected 2040–2069 100-year recurrence interval precipitation intensities under RCP 8.5 for the station at Ithaca, NY.

Typically, the confidence interval and 10th-to-90th-percentile envelope overlap, indicating that the lowest projections fall within the observed confidence interval bounds. This allows a user to view the future projections in the context of the uncertainty inherent to the historical data. It also suggests that a feasible (although lenient) adaptation requirement would be the use of the observed data's upper confidence interval bound. A more stringent criterion for considering future extreme precipitation amounts could be based on the solid line in the IDF curve. This line represents the mean intensity over the 49 climate model-downscaling-method combinations for the specified time period and concentration pathway.

In addition to the IDF curves, the website also provides more general map-based information for policy makers and other non-technical audiences. The website allows users to view maps of projected changes in precipitation extremes, as well as related maps showing the relative frequency of future precipitation events compared to the observed historical frequency (Fig. 11).

7. Summary

NYS legislation requires that state agencies, local governments and engineers account for climate change in certain planning, funding and permitting decisions. Informed by the latest collection of climate model simulations and climate data downscaling techniques, tools and quantifiable guidance for implementing CRRA in decisions affected by precipitation extremes are now available.

The outcomes of this work provide a template for other climate service providers to develop and disseminate climate-science-informed information for climate change adaptation. Although only modest increases in precipitation extremes are expected through the early part of the 21st century, substantial increases in extreme precipitation intensity are projected by the end of the century. Despite the caveats associated with the ability of AOGCMs to simulate changes in specific extreme weather events, planning for future climate resiliency requires that certain decisions be made today using the best available information concerning future changes. By understanding the uncertainly associated with both historical extreme precipitation statistics and projections of future values, policy makers can be informed by the latest climate science. However, to be most effective, an iterative process must be put in place such that recommendations and decisions are re-evaluated at set intervals based on 1) advances in climate science and modeling and 2) evaluation of past projections in light of the evolving observational climate record. Climate service providers should be prepared to assume this operational role, which differs considerably from the publication of static extreme precipitation climatologies. In NYS, such a user need is clearly articulated in CRRA's mandate that sea-level rise projections be updated at least every five years. A similar provision for extreme precipitation projections is essential.

Acknowledgments

This research was supported by the New York State Energy Research and Development Authority (Contract 28257), with partial support from NOAA Contract EA133E07CN0090 and the New York State Agricultural Experiment Station.

References

Alexander, L.V., Arblaster, J.M., 2009. Assessing trends in observed and modelled climate extremes over Australia in relation to future projections. Int. J. Climatol. 29, 417–435.

Allen, R.J., DeGaetano, A.T., 2005. Areal reduction factors for two eastern United States regions with high rain-gauge density. J. Hydrol. Eng. 10, 327–335.

AMEC Environment Infrastructure, 2012. Development of projected intensity–duration–frequency curves for Welland, Ontario, Canada (Final Report), National Engineering Vulnerability Assessment of Public Infrastructure to Climate Change City of Welland Stormwater and Wastewater Infrastructure. [Available online https://www.welland.ca/Eng/pdfs/AppC-WellandReportFinal.pdf].

Cannon, A.J., Sobie, S.R., Murdock, T.Q., 2015. Bias correction of GCM precipitation by quantile mapping: how well do methods preserve changes in quantiles and extremes? J. Clim. 28, 6938–6959.

Castellano, C.M., DeGaetano, A.T., 2015. A multi-step approach for downscaling daily precipitation extremes from historical analogues. Int. J. Climotol. 30, 1797–1807.

Collins, M., 2013. Section 12.3.1.3 The New Concentration Driven RCP Scenarios, and their Extensions. Chapter 12 Long-term Climate Change: Projections, Commitments and Irreversibility. IPCC AR5 WG1 2013, pp. 1045–1047.

Cortés-Hernández, V.E., Zheng, F., Evans, J., Lambert, M., Sharma, A., Westra, S., 2015. Evaluating regional climate models for simulating sub-daily rainfall extremes. Dyn. Clim. 10.1007/s00382-015-2923-4 doi:10.1007/s00382-015-2923-4.

Coumou, D., Rahmstorf, S., 2012. A decade of weather extremes. Nat. Clim. Change 2, 491–496.

DeGaetano, A.T., 1998. A Smirnov test-based clustering algorithm with application to extreme precipitation data. Water Resour. Res. 34, 169–176.

DeGaetano, A.T., 2009. Time-dependent changes in extreme-precipitation return-period amounts in the continental United States. J. Appl. Meteor. Climatol. 48, 2086–2099.

DeGaetano, A.T., Noon, W., Eggleston, K.L., 2015. Efficient access to climate products using ACIS Web Services. Bull. Am. Meteor. Soc. 96, 173–180.

Donat, M.G., Lowry, A.L., Alexander, L.V., O'Gorman, P.A., Maher, N., 2016. More extreme precipitation in the world's dry and wet regions. Nat. Clim. Change 6, 508–513.

Doswell, C.A., Brooks, H.E., Maddox, R.A., 1996. Flash flood forecasting: an ingredients based methodology. Weather Forecast. 11, 560–581.

Fischer, E.M., Knutti, R., 2016. Observed heavy precipitation increase confirms theory and early models. Nat. Clim. Change 6 (11), 986–991. http://dx.doi.org/10.1038/nclimate3110.

Groisman, P.Ya., Knight, R.W., Easterling, D.R., Karl, T.R., Hegerl, G.C., Razuvaev, V.N., 2005. Trends in intense precipitation in the climate record. J. Clim. 18, 1343–1367.

Groisman, P.Ya., Knight, R.W., Karl, T.R., 2012. Changes in intense precipitation over the central United States. J. Hydrometeor. 13, 47–66. http://dx.doi.org/10.1175/JHM-D-11-039.1.

Heineman, M., 2012. Trends in precipitation maxima at U.S. Historical Climatology Network stations 1893-2010. In: Proceedings World Environmental and Water Resources Congress. American Society of Civil Engineers, 2003-2012.

Hershfield, D.M., 1961. Rainfall Frequency Atlas of the United States. U.S. Weather Bureau Technical Paper 40. Department of Commerce, Washington DC.

Hirschboeck, K.K., Ely, L.L., Maddox, R.A., 2000. Hydroclimatology of meteorologic floods. Inland Flood Hazards: Human, Riparian and Aquatic Communities. Cambridge University Press, pp. 39–72.

Hosking, J.R.M., Wallis, J.R., 1997. Regional Frequency Analysis: An Approach Based on L-moments. Cambridge University Press. 244 pp.

IPCC, 2014. In: Core Writing Team, Pachauri, R.K., Myer, L.A. (Eds.), Synthesis Report: Contribution of Working Groups I, II and III to the Fifth Assessment Report of the Intergovernmental Panel on Climate Change. IPCC, Geneva, Switzerland, p. 151.

Janssen, E., Wuebbles, D.J., Kunkel, K.E., Olsen, S.C., Goodman, A., 2014. Observational- and model-based trends and projections of extreme precipitation over the contiguous United States. Earth's Future 2, 99–113. http://dx.doi.org/10.1002/2013EF000185.

Jones, C., Giorgi, F., Asrar, G., 2011. The Coordinated Regional Downscaling Experiment: CORDEX; An international downscaling link to CMIP5. CLIVAR Exchanges, No. 56, International CLIVAR Project Office, Southampton, United Kingdom, 34–40

Kalnay, E., Coauthors, 1996. The NCEP/NCAR 40-year reanalysis project. Bull. Am. Meteor. Soc. 77, 437–471.

Kenyon, J., Hegerl, G.C., 2010. Influence of modes of climate variability on global precipitation extremes. J. Clim. 23 (23), 6248–6262.

Kunkel, K.E., Andsager, K., Easterling, D.R., 1999. Long-term trends in extreme precipitation events over the conterminous United States and Canada. J. Clim. 12, 2515–2527.

Kunkel, K.E., 2003. North American trends in extreme precipitation. Nat. Hazards 29, 291–305.

Limsakul, A., Singhruck, P., 2016. Long-term trends and variability of total and extreme precipitation in Thailand. Atmos. Res. 169, 301–317.

Maddox, R.A., Chappell, C.F., Hoxit, L.R., 1979. Synoptic and meso-α scale aspects of flash flood events. Bull. Am. Meteor. Soc. 60, 115–123.

McKay, M., Wilks, D.S., 1995. Atlas of Short-Duration Precipitation Extremes for the Northeastern United States and southeastern Canada. Northeast Regional Climate Center Research Publication. RR 95-1, p. 26.

Menne, M.J., Durre, I., Vose, R.S., Gleason, B.E., Houston, T.G., 2012. An overview of the global historical climatology network-daily database. J. Atmos. Oceanic Technol. 29, 897–910.

Mielke, P.W., Johnson, E.S., 1974. Some generalized beta distributions of the second kind having desirable application features in hydrology and meteorology. Water Resour. Res. 10, 223–226.

Moberg, A., Coauthors, 2006. Indices for daily temperature and precipitation extremes in Europe analyzed for the period 1901–2000. J. Geophys. Res. 111, D22106. http://dx.doi.org/10.1029/2006JD007103.

Ning, L., Riddle, E.E., Bradley, R.S., 2015. Projected changes in climate extremes over the northeastern United States. J. Clim. 28, 3289–3310.

Palecki, M.A., Angel, J.R., Hollinger, S.E., 2005. Storm precipitation in the United States. Part I: meteorological characteristics. J. Appl. Meteorol. 44 (6), 933–946.

Perica, S., Martin, D., Pavlovic, S., Roy, I., St. Laurent, M., Trypaluk, C., Unruh, D., Yekta, M., Bonnin, G., 2013. NOAA Atlas 14: Precipitation-Frequency Atlas of the United States, Vol. 9. Prepared by the U.S. Department of Commerce, National Oceanic and Atmospheric Administration, National Weather Service, Silver Spring, MD, 43 pp.

Press, W.H., Flannery, B.P., Teukolsky, S.A., Vettering, W.T., 1986. Numerical Recipes: The Art of Scientific Computing. Cambridge University Press, p. 818.

Rodríguez, R., Navarro, X., Casas, M.C., Ribalaygua, J., Russo, B., Pouget, L., Redaño, A., 2014. Influence of climate change on IDF curves for the metropolitan area of Barcelona (Spain). Int. J. Climatol. 34, 643–654.

Scherrer, S.C., Fischer, E.M., Posselt, R., Liniger, M.A., Croci-Maspoli, M., Knutti, R., 2016. Emerging trends in heavy precipitation and hot temperature extremes in Switzerland. J. Geophys. Res. Atmos. 121, 2626–2637. http://dx.doi.org/10.1002/ 2015JD024634.

Scoccimarro, E., Villarini, G., Vichi, M., Zampieri, M., Fogli, P.G., Bellucci, A., Gualdi, S., 2015. Projected changes in intense precipitation over Europe at the daily and subdaily time scales. J. Clim. 28, 6193–6203.

Sun, Q., Miao, C., Duan, Q., 2016. Extreme climate events and agricultural climate indices in China: CMIP5 model evaluation and projections. Int. J. Climatol. 36, 43–61. http://dx.doi.org/10.1002/joc.4328.

Taylor, K.E., Stouffer, R.J., Meehl, G.A., 2012. An overview of CMIP5 and the experiment design. Bull. Am. Meteor. Soc. 93, 485–498.

Towler, E., Rajagopalan, B., Gilleland, E., Summers, S., Yates, D., Katz, R.W., 2010. Modeling hydrologic and water quality extremes in a changing climate: a statistical approach based on extreme value theory. Water Resour. Res. 46, W11504. http://dx.doi.org/10.1029/2009WR008876.

Wang, X., Huang, G., Liu, J., Li, Z., Zhao, S., 2015. Ensemble projections of regional climatic changes over Ontario, Canada. J. Clim. 28, 7327–7346.

Ward, A.D., Trimble, S.W., Burckhard, S.R., Lyon, J.G., 2015. Environmental Hydrology. CRC Press, p. 663.

Westra, S., Fowler, H.J., Evans, J.P., Alexander, L.V., Berg, P., Johnson, F., Kendon, E.J., Lenderink, G., Roberts, N.M., 2014. Future changes to the intensity and frequency of short-duration extreme rainfall. Rev. Geophys. 52, 522–555. http://dx.doi.org/10.1002/2014RG000464.

Wilks, D.S., 1993. Comparison of 3-parameter probability distributions for representing annual extreme and partial-duration precipitation series. Water Resour. Res. 29, 3543–3549.

Wilks, D.S., Cember, R.P., 1993. Atlas of Precipitation Extremes for the Northeastern United States and Southeastern Canada. Northeast Regional Climate Center Research Publication RR 93-5, p. 40.

Wilson, S., Hassell, D., Hein, D., Morrell, C., Tucker, S., Jones, R., Taylor, R., 2011. *Installing and using the Hadley Centre regional climate modelling system, PRECIS.* Met Office Hadley Centre Rep., 157 pp. [Available online at http://www.metoffice.gov.uk/media/pdf/o/5/tech_man_vn1.9.3.pdf.pdf.].

Xuereb, K., Green, J., 2012. Defining independence of rainfall events with a partial duration series approach. In: Hydrology and Water Resources Symposium 2012. Engineers Australia, p. 169.

Yarnell, D.L., 1935. Rainfall Intensity-Frequency Data, Miscellaneous Publication No. S04, U.S. Department of Agriculture, Washington, D.C., p. 68.